

A Comparison between Optimization and Filtering Techniques for RC Thermal Model Identification

Heman Shamachurn

Department of Electrical and Electronic Engineering,
Faculty of Engineering,
University of Mauritius
Reduit, Mauritius
h.shamachurn@uom.ac.mu

S Z Sayed Hassen

Department of Electrical and Electronic Engineering,
Faculty of Engineering,
University of Mauritius
Reduit, Mauritius
z.sayedhassen@uom.ac.mu

Abstract— Anticipatory control methods can enable the participation of buildings in demand-side management. Model-based control techniques offer promising avenues to improve the energy efficiency of buildings. Grey-box model identification can be carried out through optimization and filtering techniques. In this work, these two techniques were compared for the identification of a second order RC grey-box model using open-loop input-output data. It was found that, generally, the filtering method identifies the model over a shorter time period as compared to the optimization technique. Moreover, using the filtering approach, the poor initial state guesses can be taken care of, while it can be problematic to deal with this issue in an optimization-based identification method. We show then that the model may not necessarily be identified accurately but may still produce accurate simulation results. Finally, we also determine the extent to which the identified parameters drift away from their true values with increasing noise intensity in the identification data.

Keywords— grey-box model, RC model, fmincon, extended kalman filter, model identification

I. INTRODUCTION

Buildings and the building construction sectors combined together consume about one third of the global final energy use and are responsible for nearly 28 % of the energy-related CO₂ emissions [1]. Heating, Ventilation and Air-Conditioning (HVAC) systems use about 37 % of the total energy associated with buildings [2]. The energy efficiency of existing buildings can be significantly improved by upgrading the conventional energy management systems through the implementation of advanced control technologies [3]. About 30 % of energy wastage occurs in commercial buildings due to poor sensors and control systems [4]. The traditional ON/OFF and Proportional-Integral-Derivative (PID) controllers are not as effective as the model-based predictive controllers in maintaining a good energy efficiency ([5], [6]), given that they cannot perform anticipatory control, cannot allow for disturbance rejection, cannot handle constraints, and cannot deal with time-varying plant dynamics [7].

The model employed by model-based control methods should have the minimal complexity while at the same time reproduce the thermal dynamics of the building accurately. The model development stage is the most expensive and time-consuming part of a model-based control implementation

project [8], [9]. Models are generally classified into white-box, grey-box and black-box categories. They can also be of linear or non-linear types and/or time-varying or time-invariant. The emphasis of this work is on the linear, time-invariant (LTI) resistance-capacitance (RC) grey-box model identification, which is based on the electrical analogy to model the flow of heat. An extensive review pointed out that the RC parameters for thermal models of buildings have been determined through several techniques [10]. Researchers have mostly applied optimization and filtering methods for the model identification. The model's output is generally the building's indoor air temperature. The inputs typically consist of the solar irradiance, the outdoor ambient temperature, the HVAC heating/cooling power, and other disturbances such as heat gains from occupants, lighting and equipment. The literature review has not shown evidence of any research work dealing with a thorough comparison between the filtering and optimization-based identification techniques. Moreover, the Extended Kalman Filter (EKF) has not been tested under noisy data and varying initial state conditions. Therefore, this work aims to perform a comparison between an optimization-based approach and an EKF-based approach to identify a building RC thermal model under different noise and initial state conditions.

II. METHODOLOGY

A. Thermal model

The 2nd order RC thermal model used in this work is shown in Fig. 1.

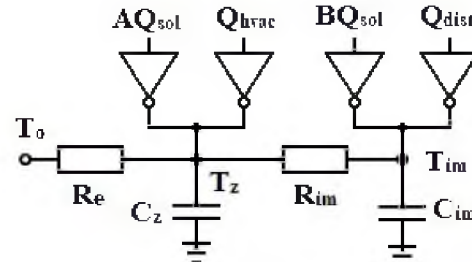


Fig. 1. 2nd order RC model

The parameters are defined as follows: T_z : Measured zone air temperature (°C), T_o : Outside air temperature (°C), T_{im} : Internal mass temperature (°C), A : Factor which decides about

the part of the Global Horizontal Irradiance (GHI) which is convective and has a direct impact on the zone air temperature (36.08 m^2), B: Factor which decides about the part of the GHI which is radiative and has a direct impact on the internal mass of the zone (56.31 m^2). The internal mass will absorb the energy first, before releasing it to the zone air, Q_{sol} : GHI (kW/m^2), Q_{hvac} : Heating/Cooling power assumed to be convective only, Q_{dist} : Disturbances (occupants, equipment and lighting) heat gain, R_e : Thermal resistance linking the outdoor air to the zone air ($0.429 \text{ K}/\text{kW}$), R_{im} : Thermal resistance linking the zone air to the internal mass in the zone ($0.128 \text{ K}/\text{kW}$), C_{im} : Thermal capacitance of the internal thermal mass ($8.39 \times 10^5 \text{ kJ}/\text{K}$), and C_z : Zone air thermal capacitance ($1.34 \times 10^5 \text{ kJ}/\text{K}$). The continuous-time dynamic model is described by equations (1) and (2).

$$C_z \dot{T}_z = \frac{T_o - T_z}{R_e} + \frac{T_{\text{im}} - T_z}{R_{\text{im}}} + A Q_{\text{sol}} + Q_{\text{hvac}} \quad (1)$$

$$C_{\text{im}} \dot{T}_{\text{im}} = \frac{T_z - T_{\text{im}}}{R_{\text{im}}} + B Q_{\text{sol}} + Q_{\text{dist}} \quad (2)$$

A continuous time (CT) state space (SS) model of the thermal zone was formulated using the dynamic equations. The state T_z was the only measurable state, and was also the output of the model. To enable the use of sampled input-output data, the CT model was discretized with a sampling time period of 5 minutes, using the zero-order hold technique, to obtain a discrete time (DT) LTI model. The model was then simulated with the typical input data shown in Fig. 2 and an initial state of $[T_z, T_{\text{im}}] = [23.5, 25]$. The model output zone temperature is also shown in Fig. 2.

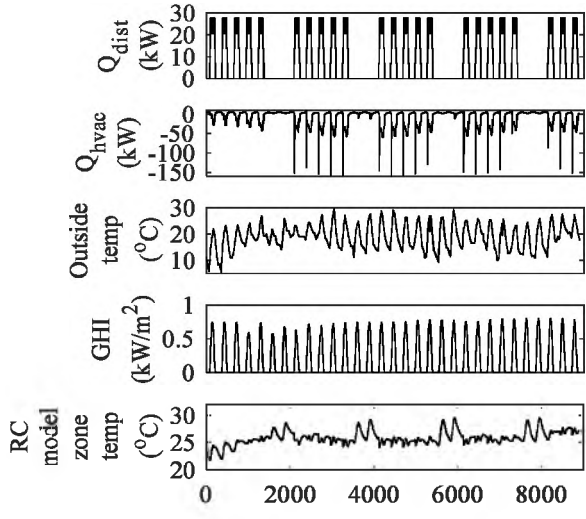


Fig. 2. Input-output data for identification

B. Optimization algorithm

The procedure is presented as follows:

1. The parameter search space is defined
2. Latin Hypercube Sampling (LHS) is used to select an initial parameter vector
3. The DT SS model matrices are calculated using the vector in 2
4. The optimization objective function is computed

5. The parameter vector is updated and steps 1-5 repeated until the stopping criterion is achieved
6. The optimum parameter vector is saved

In this work the objective was to minimize the sum of squared error (SSE) between the actual and the simulated zone temperatures. The objective was a non-convex function of the parameter vector so that, depending on the initial parameter guess (IPG), the optimization could lead to a local minimum. Therefore, steps 1-6 were applied 30 times, every time starting with a distinct IPG determined by LHS. Eventually, 30 optimal solutions were obtained. The data for the first 20 days (1st to 5760th data points) was used to identify the model, and the remaining data for about 11 days (5761st to 8900th data points) was used to test the identified model. The parameter search space was defined to be in a narrow range of $0.7 x$ to $1.3 x$, where x is the nominal parameter value provided in section II part A.

To study the impact of noisy input-output data on the identification results, random noise with reasonable standard deviations were added to the identification data. The noise standard deviations were $0.3 \text{ }^\circ\text{C}$, $0.05 \text{ kW}/\text{m}^2$, 0.5 kW and 0.4 kW for the temperatures, GHI, Q_{hvac} and Q_{dist} respectively. The noisy GHI and Q_{dist} signals were not allowed to contain negative values. The model identified using noisy data was then simulated using clean input data, and the corresponding output compared to the output of the true model.

To study the impact of the initial state guess (ISG) on the identification results, the second state T_{im} was assumed to be 20°C in 1 case and 30°C in another case, rather than the correct value of 25°C . Normally, the first state T_z is known as it is the measured model output. However, the second state cannot be measured in a practical application. Therefore, it is important to know the impact of assuming it to be a certain value. It has to be noted that this aspect has not been addressed in literature. Probably, the authors have assumed that the ISG will not have an impact on the identification results, and therefore omitted a study in this direction.

Box plots were used to investigate the physicality and the spread of the identified parameters in all the scenarios, given that an identified model may have a good simulation accuracy even though the identified parameters are different from the actual parameters and sometimes, may have no physical meaning at all.

C. EKF algorithm

The simultaneous estimation of the states and parameters is referred to as joint-estimation. Details about the equations are provided in [11]. Even if the model is linear, augmenting the state vector with the parameters yields a non-linear problem. Therefore, the non-linear KF, EKF, was used to estimate the RC parameters. For the EKF, the process error covariance (PEC) matrix was $Q = \text{diag}(10^{-4}, 10^{-4}, 10^{-20}, 10^{-20}, 10^{-20}, 10^{-20}, 10^{-20})$ for the augmented state vector $x = (T_z, T_{\text{im}}, R_e, C_z, R_{\text{im}}, C_{\text{im}}, A, B)$. The very low PEC of 10^{-20} for the parameters represent the time-invariability of the parameters. The measurement error covariance was $R = 10^{-8}$ for the case where no noise was present and was $R = 10^{-2}$ for the case where noise was present in the identification data. The error covariance (EC) matrix was $\text{cov} =$

$\text{diag}(1, 25, 0.02, 2 \times 10^9, 0.0015, 6.5 \times 10^{10}, 150, 300)$. The EC for the parameters were calculated based on the estimate of the maximum error in the initial guess. For T_z , the EC is low, given that it is a known parameter. T_{im} is not a measured quantity, so that its EC is relatively high, to consider a maximum possible error of 5°C in the assumed initial temperature. The EKF-converged parameters were calculated as the average of their values over the last 288 iterations (5473rd to 5760th data points) only, representative of a whole day's iterations.

III. RESULTS AND DISCUSSIONS

The simulation RMSE of each identified model under the different considered initial states and noisy conditions are shown for all the 30 IPGs in Fig. 3 and Fig. 4. SSE1 corresponds to an ISG of [23.5, 25], which is the correct exact initial state. SSE2 corresponds to an ISG of [23.5, 20], and SSE3 corresponds to an ISG of [23.5, 30]. The identified model 'EKF-SSE1' implies the model identified using EKF with the SSE1 as the ISG. Fig. 3 provides the results for the case when the identification data contained no noise. It can be observed that the wrongly assumed initial 2nd state (SSE2 and SSE3) tends to affect the optimization-based identification results, whereby the resulting model had a poor simulation capability. This is represented by the RMSEs for fmincon-SSE2 and fmincon-SSE3 being relatively higher compared to the other cases. However, the filter-based identified model could still achieve a reasonable simulation accuracy under these conditions, as shown by the much lower RMSEs for the EKF-SSE2 and EKF-SSE3 cases.

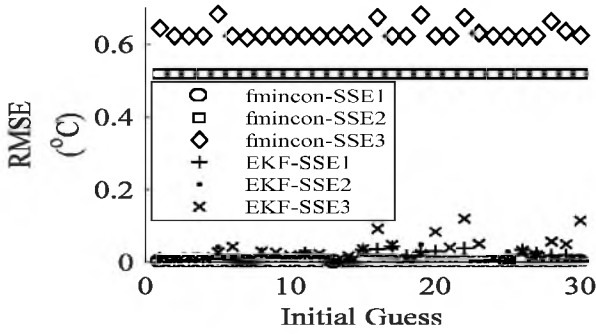


Fig. 3. Simulation RMSE - clean case

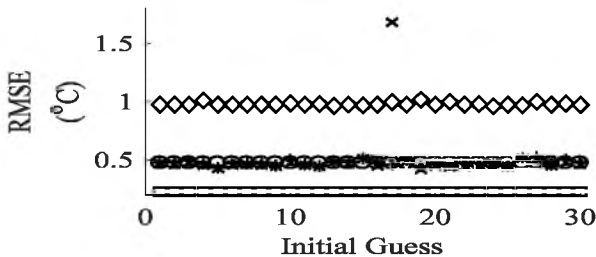


Fig. 4. Simulation RMSE - noisy case

Fig. 4 provides the results for the case where the identification data was noisy and its legend is the same as for Fig. 3. As can be observed, there is a tendency for the identified model to have a lower simulation accuracy in the presence of noise, as compared to the clean case in Fig. 3. The only anomaly occurred for fmincon-SSE2, whereby the simulation accuracy

was better for the noisy case than for the clean case. The box-plots for the different identification scenarios are shown in Fig. 5 - Fig. 10. The normalized value of each parameter was calculated as the ratio of its obtained value to its true value. Each figure reports the parameters identified for all the 30 IPGs. Optimization (fmincon)-based and filter (EKF)-based results are shown in the same figure for a better comparison. The longer horizontal bar (red) represents the median parameter. The shorter bars (black) represent the minimum and maximum values. The box (blue) represents the first quartile to the third quartile. The '+' (red) are the outliers, defined in this case as a value, which is more than 1.5 times the interquartile range away from the top or bottom of the box. Ideally, the best possible result should be just the median line located exactly at 1, with no box and with no outlier.

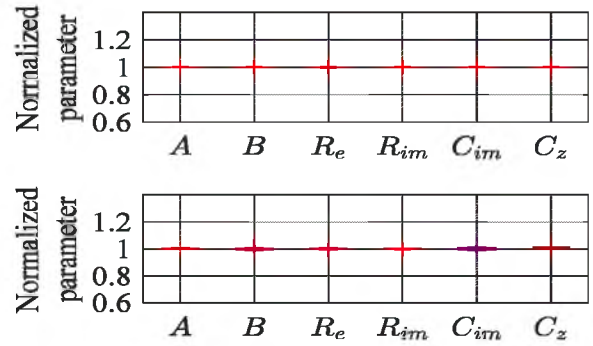


Fig. 5. Box plot for clean case - SSE1 (Top:fmincon; Bottom:EKF)

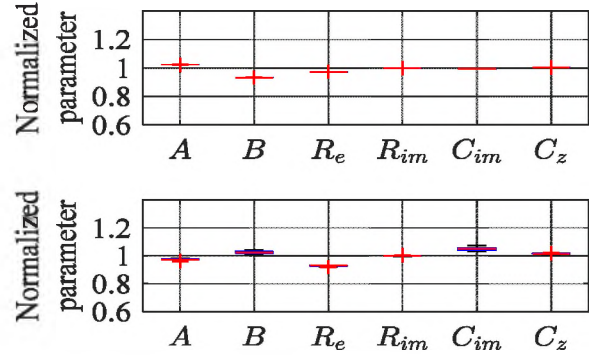


Fig. 6. Box plot for noisy case - SSE1 (Top:fmincon; Bottom:EKF)

For the clean case in Fig. 5, and for an ISG of SSE1, the parameters identified were more accurate when optimization was employed, as compared to using a filter. This can be deduced from the fact that the median parameter was closer to 1, and the spread of the parameters was lower for the optimization method. When identification was performed using noisy data, there was a tendency for the median parameter to shift away from the true parameter value, the effect being more pronounced for some parameters, in particular R_e , as shown in Fig. 6. Fig. 7 and Fig. 8 correspond to the identification scenarios for the ISG of SSE2. One immediate observation is that the optimization technique was more affected by the wrong ISG, compared to the filter-based identification. This is depicted by the median parameters for the optimization method being

quite far from their true values. However, even though the identified parameters were quite far from their actual value, it should be noted that the optimization-based identified models under the ISG condition of SSE2 produce a very good simulation accuracy as reported in Fig. 4 (fmincon-SSE2). One can deduce, therefore, that although the identified parameters may not be accurate, the resulting RC model can still produce accurate simulation results. Fig. 9 and Fig. 10 show the box-plots corresponding to the identification scenarios for the ISG of SSE3.

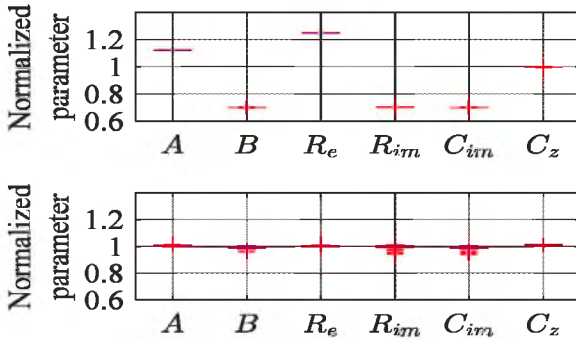


Fig. 7. Box plot for clean case - SSE2 (Top:fmincon; Bottom:EKF)

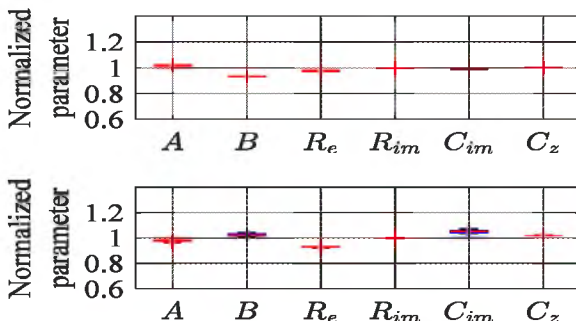


Fig. 8. Box plot for noisy case - SSE2 (Top:fmincon; Bottom:EKF)

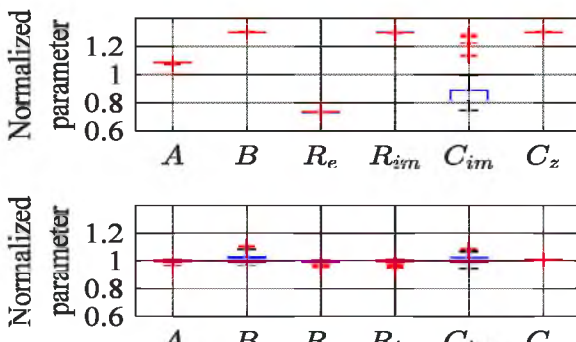


Fig. 9. Box plot for clean case - SSE3 (Top:fmincon; Bottom:EKF)

Similar observations can be made for the case of SSE3 as for the case of SSE2. For the case of SSE3, the optimization-based identification produced parameters which had medians relatively far from their true values. However, in this case, the simulation accuracies of the identified models were lower in the

presence of noise. Therefore, considering the results for the IPGs of SSE2 and SSE3, one can conclude that the unknown initial state cannot be randomly assumed in an optimization-based identification scenario as the associated impact can be significant. A filter can, on the other hand, be tuned in such a way to take into account any wrong assumption about the ISG. Even though no constraints have been imposed in the EKF algorithm, the values of the identified parameters stayed within a reasonable range as shown by the various box plots. It was noticed that the parameters B and C_{im} tended to have a larger spread, as compared to the other parameters. This could be due to the data quality and the level of excitation of each model parameter.

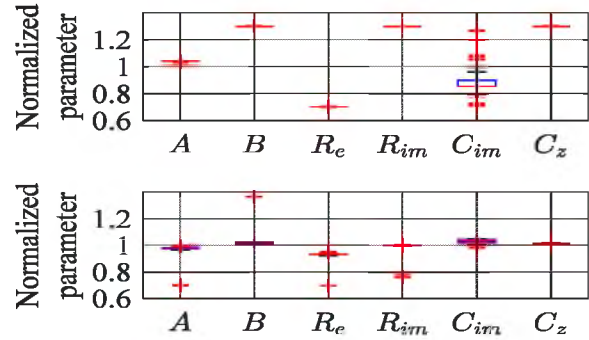


Fig. 10. Box plot for noisy case - SSE3 (Top:fmincon; Bottom:EKF)

Fig. 11-Fig. 16 compare the true model output to the outputs provided by simulating the identified models under the various scenarios (clean/noisy, ISG of SSE1/SSE2/SSE3). The results are reported for only the case where the models were identified with IPG 10. The choice for the IPG 10 was somewhat arbitrary, as the aim was to compare the waveforms provided by the models identified using the two techniques (optimization and filtering). The plots present only the validation results. Starting with the ISG, the model was simulated over the entire dataset (1st to 8900th data points). However, only the validation section (5761st to 8900th = 3140 data points) is presented in the plots.

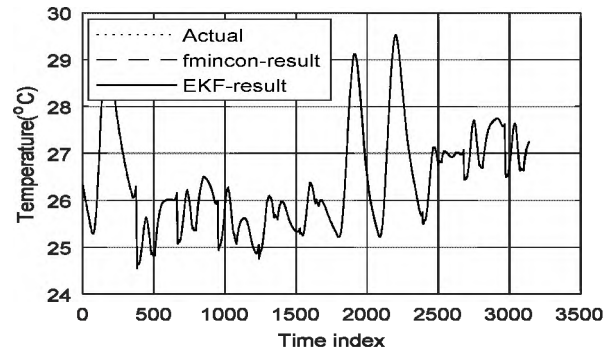


Fig. 11. Simulation of identified model - clean case - SSE1

Fig. 11 show that the model identified in the absence of noise and with an ISG of SSE1 could simulate the system with a good accuracy. When noise was present, the accuracy dropped as shown in Fig. 12. The simulated output drifted away from the true output for both identification techniques. Fig. 13 shows that, with an ISG of SSE2, the model identified using EKF had a

better simulation accuracy than the one identified using fmincon. The parameters identified using fmincon had values relatively far from the true values as shown in Fig. 7. Fig. 14 shows a drift in the waveform similar to the results in Fig. 12. Fig. 15 shows that, with an ISG of SSE3, the model identified using EKF had a better performance than the one identified using fmincon. Noise in the identification data again degraded the performance as shown in Fig. 15. It was additionally found that the optimization technique took a longer time than filter method to run for each case. For the clean data scenarios, the optimization processes took 121-147 seconds, while the filtering technique took 33 seconds for all the ISG cases.

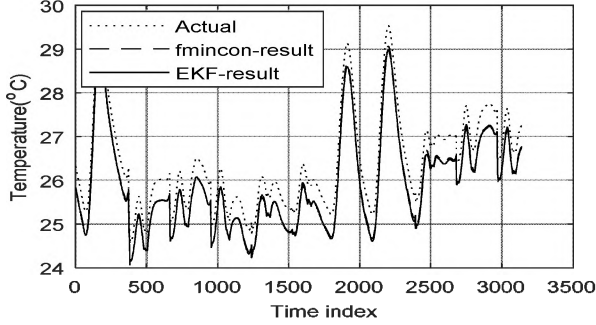


Fig. 12. Simulation of identified model - noisy case - SSE1

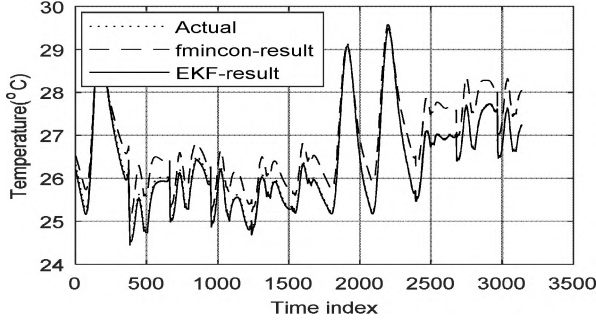


Fig. 13. Simulation of identified model - clean case - SSE2

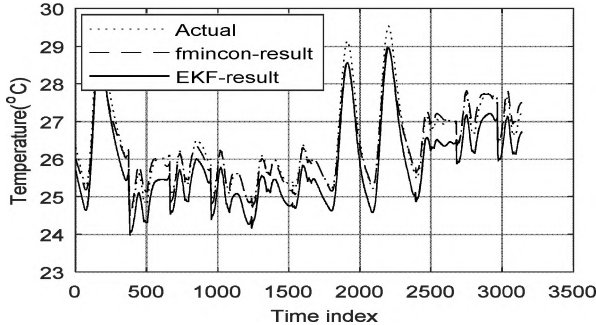


Fig. 14. Simulation of identified model - noisy case - SSE2

Fig. 17-Fig. 20 show the evolution of the normalized parameters over the successive iterations in the EKF algorithm. Fig. 17 shows that convergence occurs quite early (between the 1000th and 2000th iterations) in the absence of noise and for the ISG of SSE1. Fig. 18 and Fig. 19 show that for ISGs of SSE2 and SSE3, the EKF algorithm takes a longer time to converge,

as compared to an ISG of SSE1. Fig. 19 shows that convergence had not been completed for the two parameters C_{im} and B , even at the 5760th iteration.

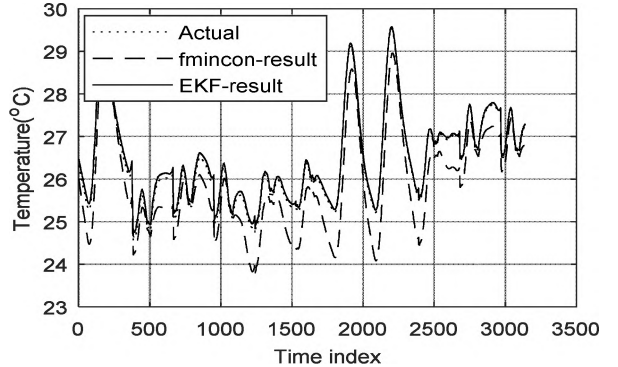


Fig. 15. Simulation of identified model - clean case - SSE3

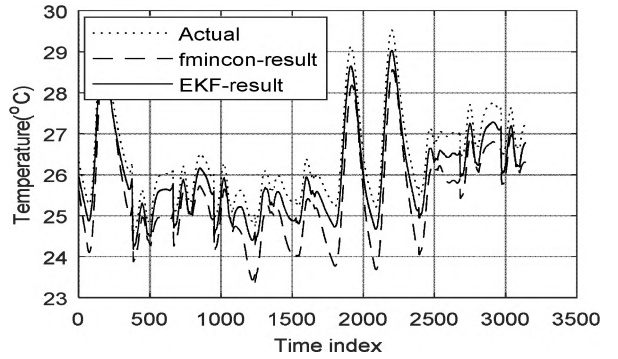


Fig. 16. Simulation of identified model - noisy case - SSE3

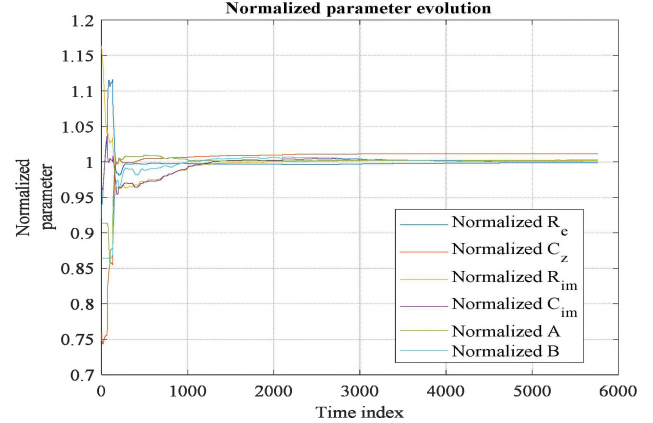


Fig. 17. Normalized parameter evolution for EKF-SSE1 - clean case

Fig. 20 shows the evolution of the normalized parameters over the successive EKF iterations for the ISG of SSE1 when noise was present in the identification data. As can be observed, the convergence did not occur smoothly, and some parameters converged to values slightly further away from their true values, as compared to Fig. 17. Moreover, the convergence took a longer time as compared to the case when no noise was present in the identification data. Similar conclusions can be drawn about the noisy SSE2 and SSE3 cases.

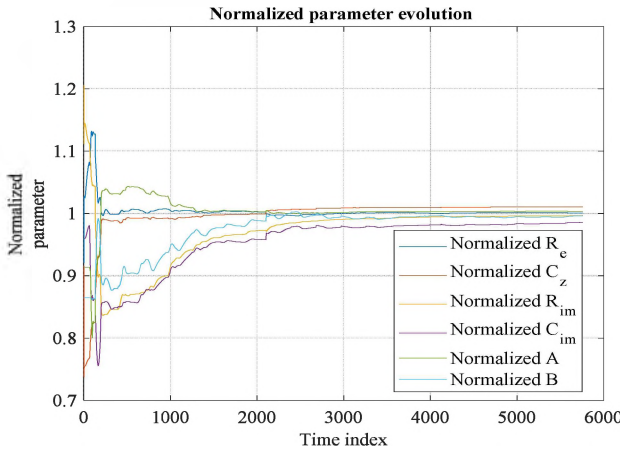


Fig. 18. Normalized parameter evolution for EKF-SSE2 - clean case

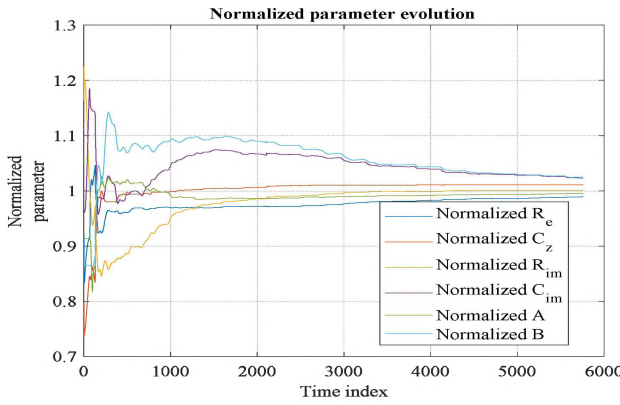


Fig. 19. Normalized parameter evolution for EKF-SSE3 - clean case

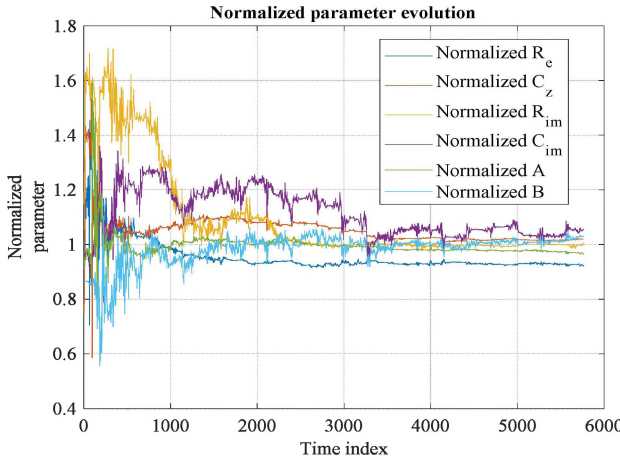


Fig. 20. Normalized parameter evolution for EKF-SSE1 - noisy case

IV. CONCLUSION

In this work, the performance of an EKF-based and an optimization based approaches to identify a building RC grey-box model were compared. The optimization technique was found to be vulnerable to the guess of the initial state, whereby some parameters were identified as being quite far from their true values. However, in one particular case, the identified

model was still able to simulate the zone temperature accurately, although the physical meaning of the parameters could be questioned. The EKF technique, on the other hand, could identify the parameters more accurately than the optimization technique in all the cases where the initial state was erroneously assumed. Moreover, the resulting identified models could produce good simulation results these cases. Furthermore, the optimization algorithm took a longer time than the EKF when identifying the parameters. For both identification methods, the identified parameters drifted away from their true values when the identification data contained noise, and the resulting simulated temperature lost accuracy. Future work will involve more detailed analyses on the length of identification data, as well as better tuning of the EKF to tackle noisy conditions.

REFERENCES

- [1] IEA, "IEA the critical role of buildings," 2019. [Online]. Available: <https://www.iea.org/reports/the-critical-role-of-buildings>. [Accessed: 05-Apr-2020].
- [2] D. Ürge-Vorsatz, L. F. Cabeza, S. Serrano, C. Barreneche, and K. Petrichenko, "Heating and cooling energy trends and drivers in buildings," *Renewable and Sustainable Energy Reviews*, vol. 41. Elsevier Ltd, pp. 85–98, 01-Jan-2015.
- [3] S. Salakij, N. Yu, S. Paolucci, and P. Antsaklis, "Model-Based Predictive Control for building energy management. I: Energy modeling and optimal control," *Energy Build.*, vol. 133, pp. 345–358, 2016.
- [4] W. Kim and S. Katipamula, "A review of fault detection and diagnostics methods for building systems," *Sci. Technol. Built Environ.*, vol. 24, no. 1, pp. 3–21, Jan. 2018.
- [5] J. Vivian, A. Zarrella, G. Emmi, and M. De Carli, "An evaluation of the suitability of lumped-capacitance models in calculating energy needs and thermal behaviour of buildings," *Energy Build.*, vol. 150, pp. 447–465, 2017.
- [6] R. De Coninck and L. Helsen, "Practical implementation and evaluation of model predictive control for an office building in Brussels," *Energy Build.*, vol. 111, pp. 290–298, Jan. 2016.
- [7] A. Afram and F. Janabi-Sharifi, "Review of modeling methods for HVAC systems," *Appl. Therm. Eng.*, vol. 67, no. 1–2, pp. 507–519, 2014.
- [8] A. Martincevic and M. Vasak, "Constrained Kalman Filter for Identification of Semophysical Building Thermal Models," *IEEE Trans. Control Syst. Technol.*, vol. PP, pp. 1–8, 2019.
- [9] E. Atam and L. Helsen, "Control-Oriented Thermal Modeling of Multizone Buildings: Methods and Issues: Intelligent Control of a Building System," *IEEE Control Syst.*, vol. 36, no. 3, pp. 86–111, 2016.
- [10] Z. Wang and Y. Chen, "Data-driven modeling of building thermal dynamics: Methodology and state of the art," *Energy Build.*, vol. 203, 2019.
- [11] S. F. Fux, A. Ashouri, M. J. Benz, and L. Guzzella, "EKF based self-adaptive thermal model for a passive house," *Energy Build.*, vol. 68, no. PART C, pp. 811–817, 2014.